Characterization and Application of Nanomaterials 2026, 9(1), 026180010.
https://doi.org/10.24294/can026180010

Article

Design and TCAD simulation of a self-powered UV photodetector based on a multilayer graphene/ZnO nanowires heterostructure for wearable and biomedical applications

Shonak Bansal[1]*, Krishna Prakash[2], Payal Patial[1], Anupma Gupta[1]

[1] Department of Electronics and Communication Engineering, Chandigarh University, Mohali 140413, India
[2] Department of Information and Communication Technology, Marwadi University, Rajkot 360003, India
* **Corresponding author:** Shonak Bansal, shonakk@gmail.com

CITATION

Bansal S, Prakash K, Patial P, Gupta A. Design and TCAD simulation of a self-powered UV photodetector based on multilayer graphene/ZnO nanowires heterostructure for wearable and biomedical applications. Characterization and Application of Nanomaterials. 2026; 9(1): 026180010. https://doi.org/10.24294/can026180010

ARTICLE INFO

Received: 27 April 2026
Accepted: 08 June 2026
Available online: 1 July 2026

Abstract: This work describes the design and TCAD-based simulation of a high-speed self-powered ultraviolet (UV) photodetector based on a heavily p-type doped multi-layer graphene (p^+-MLG) and lightly n-type doped ZnO nanowires (n^--ZnO NWs) heterojunction. The device structure is based on the utilization of the high built-in electric field across the heterointerface for effective carrier separation to support both self-biasing and photoconductive operations. Simulated outcomes show rectifying characteristics with a dark-mode and light-mode rectification ratios of 8.5×10^3 and 5.2×10^2, respectively. Spectral response demonstrates a maximum photocurrent-to-dark current ratio at 350 nm. The device has an external quantum efficiency (*QE*) of 55.43%, maximum responsivity (R_i) of 0.16 A/W, detectivity (D^*) of 2.44 $\times$ 10^9 Jones, and rapid photoswitching times with both rise time and fall time of 0.16 ns. Compared to previously reported graphene/ZnO photodetectors, the proposed heterostructure demonstrates enhanced photoswitching speed and efficient self-powered operation due to the optimized heterojunction design and strong internal electric field. p^+-MLG/n^--ZnO NWs integration facilitates UV detection with mechanical flexibility and low power consumption, which makes the device of great interest for wearable and biomedical sensing devices.

Keywords: dark current density; graphene; nanowire; quantum efficiency; responsivity; ultraviolet; ZnO

1. Introduction

The growing demand for flexible and self-powered electronic devices has accelerated the requirement for high-performance and energy-efficient photodetectors, especially for wearable health monitoring and biomedical diagnostic applications. Among the several spectral regimes, ultraviolet (UV) photodetection is important for skin exposure monitoring, real-time biosensing, early disease diagnosis, and environmental UV radiation monitoring [1]. Nonetheless, conventional UV photodetectors tend to be power-dependent, have bulky form factors, and lack flexibility, hence limiting their integration in contemporary wearable systems.

The recent developments in nanomaterials have created new avenues to bypass these limitations. Zinc oxide (ZnO) nanowires (NWs), possessing a wide bandgap of ~3.37 eV, high UV absorption, biocompatibility, and facile vertical growth, have appeared as a promising material for UV detection [2,3]. While all this time, two-dimensional (2D) materials like multi-layer graphene (MLG) provide high optical transparency, large carrier mobility, and mechanical flexibility [4]. When combined in a heterojunction structure, MLG and ZnO NWs can create a self-powered

photodiode that functions without external bias by using the built-in electric field at the junction [3,5,6].

In this work, a self-powered UV photodetector from a p^+-doped MLG and n^--doped ZnO NWs heterostructure by utilizing three-dimensional (3D) Silvaco TCAD simulation is proposed. The proposed photodetector shows improved photodetection performance with ultra-fast switching time and good rectification behavior under UV light. Such properties are highly desirable for biomedical and wearable applications where mechanical flexibility, low power consumption, and miniaturization are critical. The device can be incorporated into skin-mounted UV monitors, implantable diagnostic devices, and real-time biosensors for physiological parameters for continuous health monitoring and early disease diagnosis. This work demonstrates the potential of 2D/1D hybrid nanostructures for the development of future photodetectors for integrated bio-optoelectronic systems.

2. Device design and methodology

The proposed photodetector is a vertically stacked p^+-MLG/n^--ZnO NWs heterostructure designed to operate effectively in both self-powered and photoconductive modes. As illustrated in **Figure 1a**, the device consists of a thin n^--ZnO seed layer (~10 nm) at the bottom, followed by vertically aligned ZnO NWs of ~1500 nm in length and 200 nm in diameter. A p^+-MLG layer (~6 layers) is then deposited over the NWs, forming an efficient heterojunction for charge separation. Aluminum serves as the material for both the anode and the cathode, providing ohmic electrical contact.

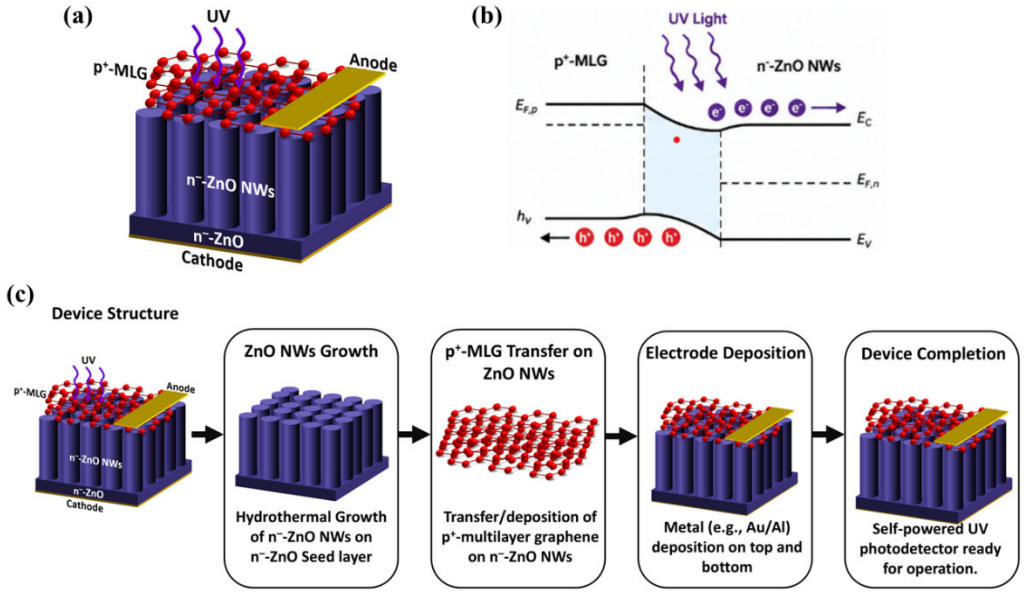

Figure 1. (**a**) The 3D schematic of p^+-MLG/n^--ZnO heterostructure photodetector. photodetector. (**b**) Energy band diagram illustrating carrier generation and separation under UV illumination. (**c**) Conceptual illustration of the representative device realization steps, included to provide physical insight into the simulated structure.

The energy band alignment and carrier transport mechanism under UV illumination are depicted in **Figure 1b**. The absorption of photons with energy larger

than the bandgap of ZnO generates electron-hole pairs in the ZnO NWs. The separation of the carriers is facilitated by the built-in electric field at the p^+-MLG/n^--ZnO interface, with the electrons drifting towards the ZnO side and the holes being transported through the graphene layer, resulting in a photocurrent generation even without any bias.

The corresponding conceptual realization route of the photodetector device is shown in **Figure 1c**, where the sequential formation of the ZnO NWs, the integration of the graphene layers, and the electrode definition are shown. This representation gives a physical insight into the device configuration and complements the TCAD-based analysis of its optoelectronic behavior. The proposed MLG/ZnO heterostructure shows a high built-in electric field arising from the difference in the Fermi levels, responsible for the efficient carrier separation and rectifying behavior.

The proposed MLG/ZnO heterostructure generates a strong built-in electric field due to the Fermi-level difference, which is responsible for efficient carrier separation and rectifying behavior. The vertically aligned ZnO NWs provide a high surface-to-volume ratio, leading to enhanced UV light absorption and facilitating fast carrier transport, whereas MLG provides high mobility, transparency, and mechanical flexibility, suitable for wearable and biomedical applications.

Simulation was conducted with Silvaco TCAD within a 3D platform to study the device's optoelectronic operation at 300 K. Simulation utilizes the drift-diffusion transport model, in combination with Poisson's equation and carrier continuity equations. Major recombination processes, including Shockley-Read-Hall, Auger, and optical recombination, are to incorporate realistic carrier physics.

The material properties employed in the simulation were obtained from various theoretical and experimental studies [3,5–9]. For p^+-MLG, bandgap of 0.25 eV, electron mobility of 40,000 $cm^2/V{\cdot}s$, and doping concentration of 2×10^{22} cm^{-3} were considered during the simulation. For n^--ZnO, a bandgap of 3.37 eV, electron mobility of 60 $cm^2/V{\cdot}s$, and doping concentration of 10^{16} cm^{-3} were taken. The simulation configuration also simulated the light source as top-incident UV at 350 nm of intensity 1 W/cm^2, considering performance under self-biasing (i.e., 0 V) and photoconductive (i.e., reverse-biased) operating conditions.

This combined modeling process offers insight into the carrier behavior, electric field distribution, and photocurrent response, confirming the suitability of the device for low-power real-time UV detection in flexible, skin-mounted biomedical devices.

Although the present study is based on TCAD simulation, the proposed p^+-MLG/n^--ZnO NW heterostructure can be experimentally realized using established nanofabrication approaches reported in recent studies [10–14]. Vertically aligned ZnO NWs can be synthesized using chemical bath deposition [15], molecular beam epitaxy [16], and electrochemical deposition [17], electron beam evaporation [18], sol-gel growth [19], and hydrothermal or vapor-phase growth techniques [20–23] on a ZnO seed layer, followed by the transfer or deposition of multilayer graphene to form the heterojunction interface. Standard lithography and metal deposition processes may then be employed to define electrical contacts and complete the device fabrication [24,25]. However, practical implementation may involve several challenges, including maintaining uniform nanowire alignment, minimizing interface defect states, preserving graphene quality during transfer, and achieving stable low-resistance

contacts. In addition, large-area integration and mechanical durability under repeated bending conditions are important considerations for wearable and biomedical applications. Future work will focus on the experimental fabrication and morphological characterization of the proposed heterostructure using SEM and TEM techniques to verify its structural integrity and validate the simulated optoelectronic performance under practical operating conditions.

3. Results and discussion

Under UV exposure, the heterostructure formed by MLG and ZnO NWs facilitates efficient photogeneration and carrier separation. The MLG layer, which is highly transparent and has a tunable Fermi level, allows the UV light to penetrate into the ZnO NWs that are the main absorbers due to their large bandgap. Photons with energy higher than the NWs bandgap excite electron-hole pairs in these nanostructures, and the internal electric field at the MLG/ZnO interface separates these photoexcited carriers. Electrons are driven towards the side of the ZnO NWs while holes are trapped in the MLG, which results in net photocurrent. The vertically stacked NWs also trap light, reducing the reflection losses, which results in high responsivity and fast carrier collection.

Figure 2 shows the current-voltage (*I-V*) characteristics of the p^+-MLG/n^--ZnO heterostructure photodetector. The photodetector exhibits rectifying behavior, with a current rectification ratio of 8.5×10^3 at ±0.5 V in the dark and 5.2×10^2 under UV illumination (λ = 350 nm, 1 W/cm^2), demonstrating diode-like performance and good charge-carrier separation across the heterostructure. Under UV illumination, the device exhibits photovoltaic characteristics in self-powered mode, achieving a photocurrent (I_{light}) of 1.2 nA/cm² and a dark current (I_{dark}) of 5×10^{-15} A/cm². This results in an outstanding I_{light}/I_{dark} ratio of 2.5×10^5, indicating high sensitivity. Under −0.5 V reverse bias, the I_{light} rises to 1.5 nA/cm² due to increased carrier drift in higher electric fields.

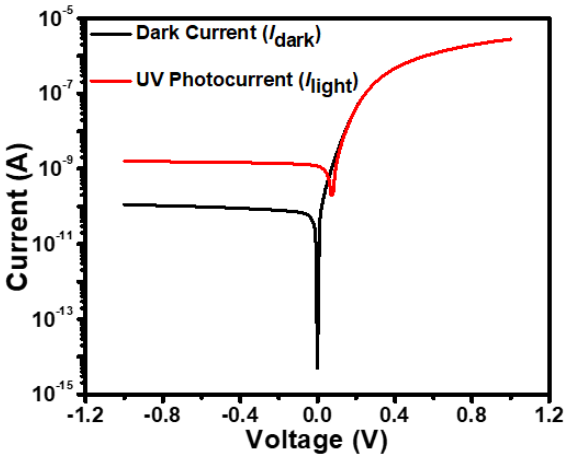

Figure 2. The simulated *I-V* characteristics of p^+-MLG/n^--ZnO heterostructure photodetector.

The variation of I_{light}/I_{dark} ratio with respect to incident wavelength (λ) at a bias of 0 and –0.5 V is shown in **Figure 3**. The ratio peaks at 350 nm because the photocurrent

is maximally generated and then decreases with increasing wavelength. In addition, an increase in reverse bias results in a decrease in I_{light}/I_{dark} ratio, which is mainly because of an increase in dark current [6].

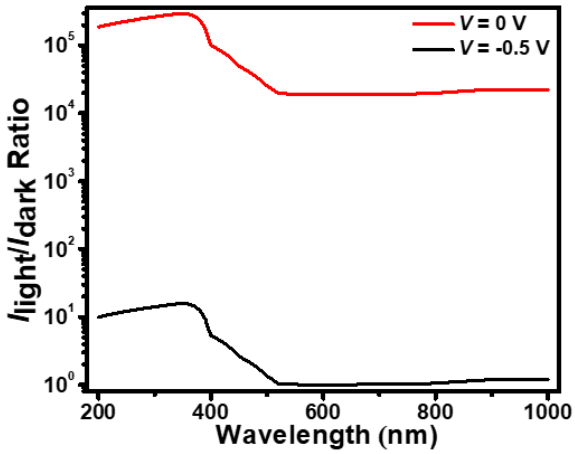

Figure 3. The I_{light}/I_{dark} Ratio-Wavelength response of p^+-MLG/n^--ZnO NWs heterostructure photodetector at 0 and –0.5 V.

Moreover, to estimate the self-biasing and photoconductive photodetection behaviour of the photodetector, the Current-Time characteristics were measured at λ = 350, 480, and 800 nm, each with the same illumination intensity at 0 and –0.5 V bias, and are shown in **Figure 4**. As illustrated in **Figure 4**, the increase in reverse bias voltage leads to a higher value of I_{light}. Furthermore, I_{light} decreases with increasing wavelength, showing the highest values at 350 nm: 1.14 nA under self-biasing and 1.42 nA under photoconductive mode. This is due to the reduced absorbance and higher optical transmittance of longer-wavelength light, indicating that light beyond a specific wavelength is minimally absorbed by the n^--ZnO NWs. The photodetector shows fast photoswitching behavior, with a rise time and fall time of 0.2 ns at 0 V and 0.16 ns at −0.5 V, confirming its high-speed operation. These rapid response times are superior to many previously reported photodetectors [26–28]. These results are consistent with the strong built-in field and short carrier transit paths in the nanowire geometry.

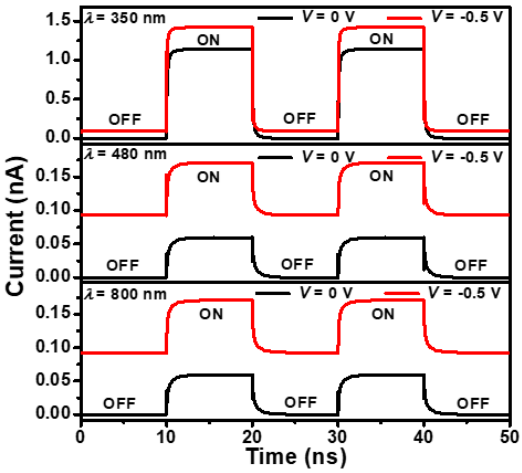

Figure 4. Current-Time characteristics of p^+-MLG/n^--ZnO NWs heterostructure photodetector at illumination wavelengths of 350, 480, and 800 nm under 0 and −0.5 V bias conditions.

To further investigate the electrical characteristics of the proposed p^+-MLG/n^- ZnO NWs heterostructure photodetector, the dynamic device resistance and capacitance were analyzed as a function of the applied bias voltage V, as shown in **Figures 5** and **6**, respectively. The dynamic device resistance (R_d) was extracted from the simulated *I-V* characteristics (**Figure 2**) using

$$R_d = \left(\frac{dI}{dV}\right)^{-1} \quad (1)$$

The effective device resistance decreases under UV illumination compared to dark conditions, indicating enhanced carrier generation and improved charge transport across the heterojunction. The reduction in resistance under illumination facilitates efficient carrier collection and contributes to the observed increase in photocurrent. In contrast, the higher resistance observed under dark conditions is associated with the limited availability of free charge carriers within the device.

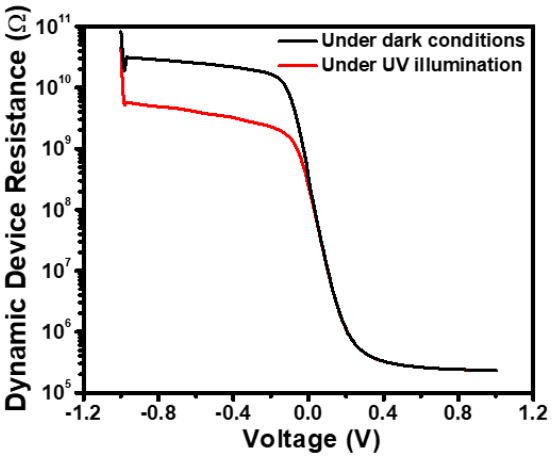

Figure 5. Dynamic device resistance-Voltage characteristics of p^+-MLG/n^--ZnO NWs heterostructure photodetector.

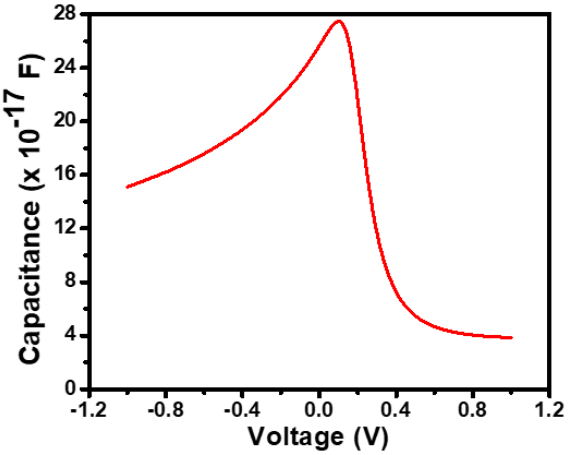

Figure 6. Capacitance-Voltage characteristics of p^+-MLG/n^--ZnO NWs heterostructure photodetector measured at a frequency of 1 MHz.

The capacitance-voltage characteristics provide additional insight into the junction behavior of the proposed heterostructure photodetector. The junction capacitance can be expressed as

$$C = \frac{\varepsilon A}{W} \tag{2}$$

where ε is the permittivity of the depletion region, A is the junction area, and W is the depletion region width. As shown in **Figure 6**, the measured capacitance at a frequency of 1 MHz gradually increases with applied bias due to the reduction in depletion width across the heterojunction interface. A maximum capacitance of approximately 27.47×10^{-17} F is observed near the low forward-bias region, after which the capacitance decreases with further increase in forward bias. This behavior may be attributed to the redistribution of charge carriers within the junction region under higher bias conditions. The relatively low capacitance values are advantageous for minimizing *RC*-delay effects and support the ultrafast transient response characteristics observed in the proposed photodetector.

In practical device implementation, contact resistance at the electrode/semiconductor interfaces and parasitic capacitances associated with the heterojunction and device geometry can influence carrier transport and switching behavior. Although ideal contact conditions were considered in the present TCAD simulation to evaluate the intrinsic characteristics of the proposed structure, the obtained resistance and capacitance characteristics provide useful insight into the possible influence of these non-ideal effects on device performance. Optimization of contact interfaces and device geometry during experimental realization would be beneficial for minimizing parasitic losses and preserving the high-speed operation of the photodetector.

To further investigate the low-noise performance of the proposed p^+-MLG/n^--ZnO NWs heterostructure photodetector, the Johnson-Nyquist thermal noise current, shot (quantum) noise current, and total noise current were analyzed as a function of applied bias voltage, as illustrated in **Figure 7**. The Johnson-Nyquist thermal noise current ($i_{thermal}$), shot noise current (i_{shot}), and total noise current (i_{total}) were estimated using the relations [29–31]:

$$i_{\text{thermal}} = \sqrt{\frac{4kT\Delta f}{R_{\text{d}}}} \tag{3}$$

$$i_{\text{shot}} = \sqrt{2q(I_{\text{dark}} + I_{\text{light}})\Delta f} \tag{4}$$

$$i_{\text{total}} = \sqrt{i_{\text{thermal}}^2 + i_{\text{shot}}^2} \tag{5}$$

where k is the Boltzmann constant, T is the absolute temperature, Δf is the bandwidth considered to be 1 Hz in this work, and q is the electronic charge.

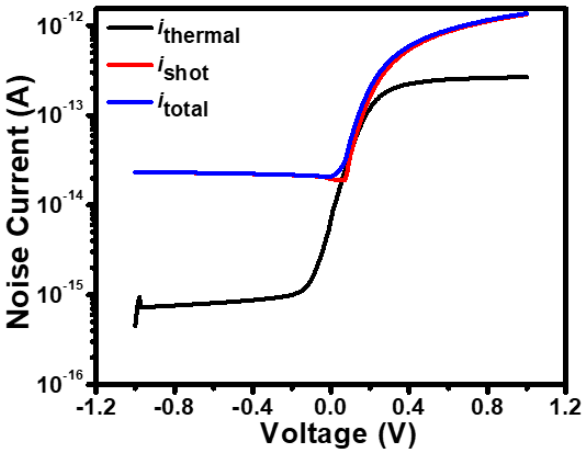

Figure 7. Variation of Johnson-Nyquist thermal noise current, shot noise current, and total noise current of the p^+-MLG/n^--ZnO NWs heterostructure photodetector as a function of applied bias voltage.

The signal-to-noise ratio (*SNR*) is an important parameter for assessing the capability of a photodetector to distinguish useful photo-generated signals from background noise [30]. A higher *SNR* corresponds to improved signal quality and detection sensitivity, enabling reliable operation under weak illumination conditions. The *SNR* is calculated using the following expression:

$$SNR(\text{dB}) = 20\log\left(\frac{I_{\text{light}}}{i_{\text{total}}}\right) \tag{6}$$

Figure 8 illustrates the variation of *SNR* with applied bias voltage. As shown in **Figure 8**, the *SNR* remains nearly constant under reverse-bias conditions, exhibits a minimum near zero bias, and subsequently increases significantly with forward bias. The enhanced *SNR* at higher forward voltages is attributed to the substantial increase in photocurrent relative to the total noise current, demonstrating the strong signal discrimination capability of the proposed photodetector. At 0 V and −0.5 V bias, the total noise currents are found to be 2.07×10^{-14} A and 2.25×10^{-14} A, respectively. The corresponding SNR values are 95.16 dB and 96.40 dB, demonstrating excellent signal discrimination capability and low-noise operation under both self-powered and reverse-bias conditions.

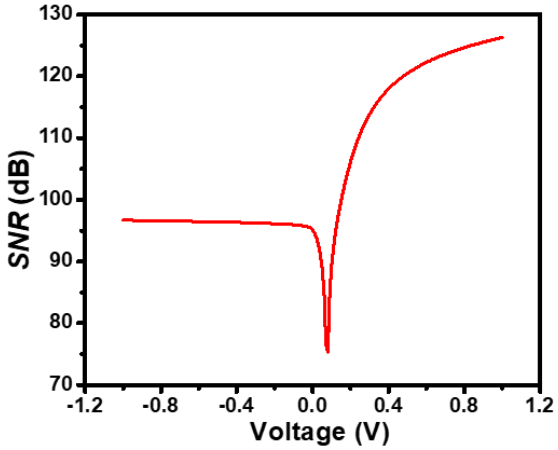

Figure 8. Variation of *SNR* of the p^+-MLG/n^--ZnO NWs heterostructure photodetector as a function of applied bias voltage.

As is clear from **Figure 7**, the Johnson-Nyquist thermal noise current remains relatively low under reverse-bias conditions because of the high effective device resistance and low dark current characteristics of the heterostructure photodetector. With increasing forward bias, the thermal noise current increases because of enhanced carrier transport across the junction region. Similarly, the shot noise current gradually increases with applied voltage due to the increase in carrier injection and current flow through the device. Consequently, the total noise current also increases with forward bias and is primarily governed by the combined contribution of thermal and shot noise mechanisms. The relatively low overall noise level observed under reverse-bias operation supports the high detectivity and low noise equivalent power (*NEP*) values obtained for the proposed photodetector, indicating its suitability for low-intensity UV sensing and high-speed photodetection applications.

In addition to thermal and shot noise, low-frequency flicker noise may also influence practical device operation, particularly during long-duration sensing conditions. However, detailed flicker noise modeling generally requires experimental characterization of interface trap states, carrier fluctuation mechanisms, and material defects, which is beyond the scope of the present TCAD-based investigation.

Figure 9 shows the spectral response (i.e., I_{light}-λ) at 0 and –0.5 V bias. The spectral response increases with reverse bias voltage, reaching a maximum at the cut-off wavelength of 350 nm, which corresponds to the intrinsic bandgap of ZnO in the UV region. The spectral response of the device increases with increasing bias voltage due to enhanced carrier separation and reduced recombination losses. A higher electric field improves the drift of photogenerated carriers toward the electrodes, resulting in a stronger photocurrent. Consequently, the overall responsivity and spectral sensitivity of the device are significantly improved under higher bias conditions.

Figures 10–12 illustrate the variation of optical characteristic parameters-external quantum efficiency (*QE*), responsivity (R_i), and detectivity (D^*) with wavelength at 0 and –0.5 V bias, respectively. The maximum optical response is observed in the wavelength region where the incoming photon energy exceeds the bandgap of the semiconductor material. The photodetector demonstrates a *QE* of 44.05 (55.43)%, a peak R_i of 0.12 (0.16) A/W, and a peak D^* of 1.94×10^9 (2.44×10^9) Jones

at 0 (–0.5) V bias. The corresponding *NEP* values are found to be 5.58 × 10^{-14} and 4.43 × 10^{-14} W/$Hz^{1/2}$ at 0 and −0.5 V bias, respectively, indicating good low-noise detection capability of the proposed photodetector.

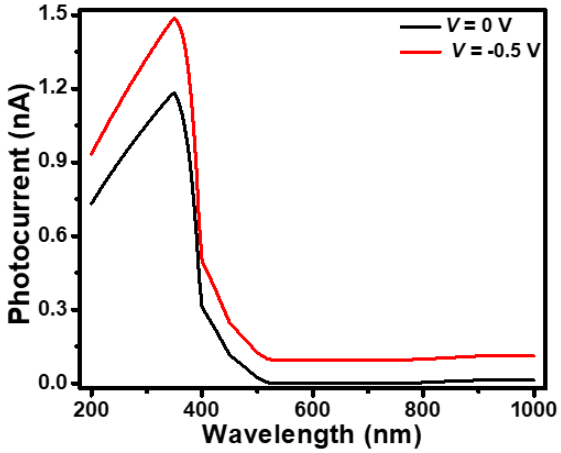

Figure 9. Spectral response characteristics of p^+-MLG/n^--ZnO NWs heterostructure photodetector at 0 and –0.5 V.

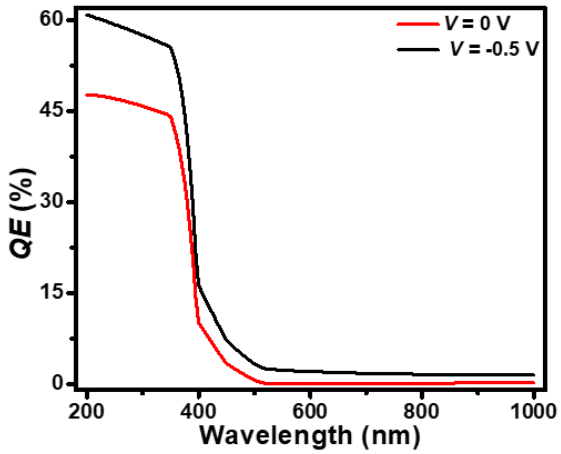

Figure 10. *QE*-Wavelength characteristics of p^+-MLG/n^--ZnO NWs heterostructure photodetector at 0 and –0.5 V.

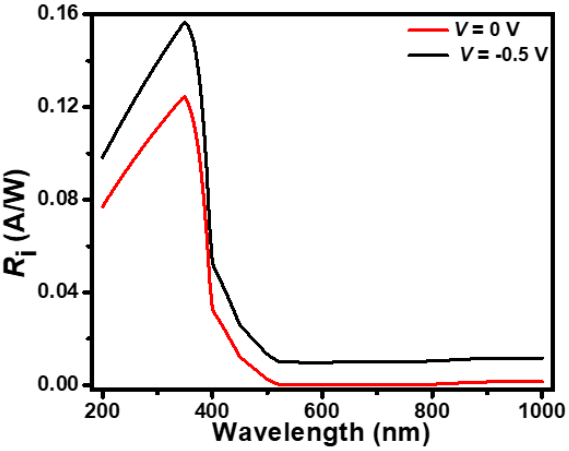

Figure 11. R_i-Wavelength characteristics of p^+-MLG/n^--ZnO NWs heterostructure photodetector at 0 and –0.5 V.

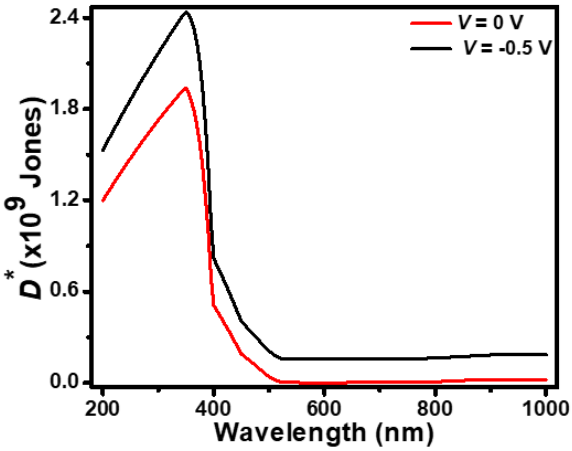

Figure 12. D^*-Wavelength characteristics of p^+-MLG/n^--ZnO NWs heterostructure photodetector at 0 and –0.5 V.

The decrease in *QE*, R_i, and D^* with increasing wavelength can be due to an increase in the rate of charge-carrier recombination at lower photon energies. The overall device performance is governed by the highly optimized nanowire array architecture, the strong built-in electric field at the heterojunction, and the high carrier mobility of the graphene layers. These features enable efficient carrier separation, fast transport, and low-power operation. For wearable and biomedical applications, long-term operational stability and mechanical reliability are also important considerations. The proposed p^+-MLG/n^--ZnO NW heterostructure is expected to exhibit good environmental stability because of the chemical robustness and electrical stability of graphene and ZnO-based materials. However, practical degradation mechanisms may arise from interface trap formation, adsorption of oxygen and moisture, contact degradation, and repeated mechanical deformation during bending or flexing. Variations in humidity and temperature may additionally influence surface charge states and photocurrent stability in ZnO nanostructures. Nevertheless, the vertically aligned nanowire geometry together with the flexible graphene layer is expected to provide improved strain accommodation and mechanical adaptability for flexible electronics applications [10,11,32]. Future work will focus on detailed experimental investigations involving long-term stability analysis, cyclic bending measurements, and environmental reliability characterization under practical operating conditions.

To further evaluate the performance of the device, a comparison with recently reported graphene/ZnO-based photodetectors is presented in **Table 1**. As can be seen from Table 1, the proposed p^+-MLG/n^--ZnO NWs heterostructure presents a balanced performance in terms of responsivity, detectivity, and ultrafast response time. Although some previously reported devices showed higher responsivity or detectivity, they suffered from slower response speeds or complex device architectures. In contrast, the proposed device exhibits nanosecond-scale switching response along with self-powered operation, making it highly suitable for real-time wearable and biomedical sensing applications. The practical applicability of the proposed photodetector is illustrated in **Figure 13**. Owing to its self-powered operation, high sensitivity, and ultrafast response, the device is well-suited for wearable UV sensing applications, enabling continuous exposure monitoring with low power consumption. In addition,

the compact heterostructure design and efficient carrier transport properties make the device suitable for biomedical sensing applications, such as real-time diagnostics and physiological monitoring. The obtained simulated results, including high responsivity, detectivity, and fast switching characteristics, support the suitability of the proposed device for next-generation flexible optoelectronic applications [33].

Table 1. Performance comparison of the proposed p^+-MLG/n^--ZnO NWs heterostructure UV photodetector with earlier reported graphene/ZnO-based photodetectors.

Structure	R_i (A/W)	D^* (Jones)	Response Time	Self-powered	Key Remarks	Ref.
p^+-Few-layer graphene/n^--ZnO NWs	0.12–0.20	~2.4×10^9	0.26–0.16 ns	Yes	TCAD-based, dual-mode operation, and analytical modeling	[6]
Hybrid NW/graphene/ZnO nanoparticles	0.79	35.68×10^6	Not reported	No	Enhanced carrier collection	[10]
GNR heterojunction	~1.04	2.45×10^{12}	310 µs	Yes	Extremely high gain but slower	[14]
NiO/ZnO heterojunction	8.6	Not reported	Not reported	Yes	Self-powered oxide PD	[32]
ZnO:Ga NWs	~0.233	4.18×10^{12}	159 ms/150 ms	Yes	High detectivity via doping	[34]
ZnO undoped	~0.074	7.79×10^{11}	222 ms/310 ms	Yes	UV detection is limited by carrier recombination	[34]
p^+-MLG/n^--ZnO NWs	0.16	2.44×10^9	0.16 ns	Yes	Ultrafast + simple heterojunction	This Work

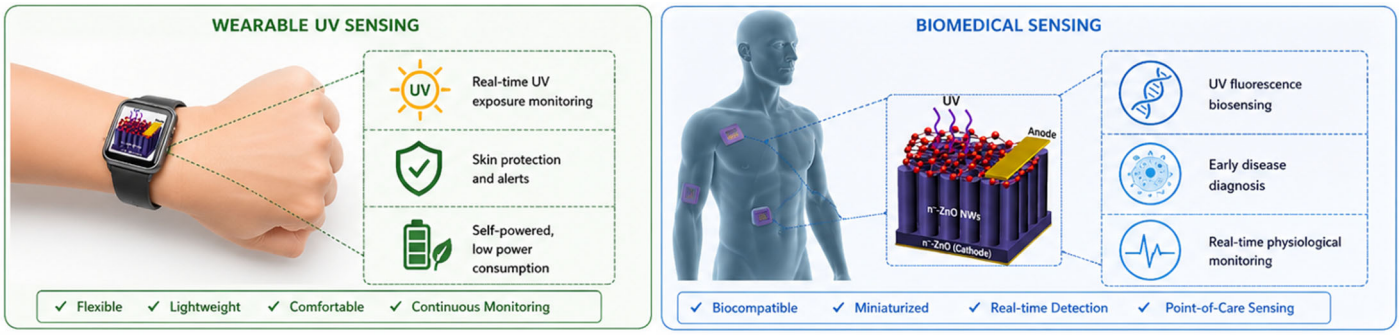

Figure 13. Potential applications of the proposed p^+-MLG/n^--ZnO NWs heterostructure photodetector in wearable UV sensing and biomedical monitoring systems.

For practical wearable and biomedical deployment, environmental and mechanical reliability are also important factors. Variations in operating temperature may affect carrier mobility, recombination characteristics, and junction transport behavior, thereby influencing the photoresponse of the device [33,35]. Similarly, adsorption of oxygen and moisture molecules on the ZnO nanowire surface under humid environments may modify the surface charge states and influence the stability of the photocurrent during long-duration operation. In addition, repeated bending conditions may introduce interface strain and contact degradation, which can affect carrier transport across the heterojunction [33,35]. Nevertheless, the flexible graphene layer together with the vertically aligned ZnO nanowire structure is expected to provide improved mechanical adaptability and structural stability for flexible sensing

applications. Future work will focus on detailed experimental investigation of temperature stability, humidity effects, and cyclic bending reliability under practical operating conditions.

4. Conclusion

In summary, a highly optimized TCAD-based design and analysis of a self-powered UV photodetector based on a p^+-MLG/n^--ZnO NWs heterostructure is presented. Vertical architecture, which involves highly transparent and conductive MLG combined with UV-sensitive ZnO NWs, enables efficient photogeneration and ultrafast carrier separation owing to a high built-in electric field at the heterointerface. The device shows excellent performance properties, including high levels of rectification, significant photocurrent responsivity, and very fast response times, thereby demonstrating its suitability for high-speed optoelectronic applications.

In addition to its optoelectronic properties, the material's flexibility, along with its miniaturized and microscale dimensions, makes it a promising candidate for integration into wearable electronic devices and biomedical monitoring systems. These findings demonstrate the potential of hybrid 2D/1D nanostructures to contribute to next-generation low-power photodetection technologies.

Author contributions: Conceptualization, methodology, writing-original draft preparation: SB; software, validation, and formal analysis: KP; investigation, data curation: PP; writing-review and editing, and visualization: AG. All authors have read and agreed to the published version of the manuscript.

Conflict of interest: The authors declare no conflict of interest.

References

1. Liu S, Wang X, Xu N, Li R, Ou H, Li S, et al. A flexible and wearable photodetector enabling ultra-broadband imaging from ultraviolet to millimeter-wave regimes. Advance Science. 2024, 11: 2401631–2401631.
2. Bansal S, Kumar S, Gupta N, Singh AK. A highly efficient and low noise n^+-ZnO/p-Si heterojunction based UV detector. In: Proceedings of the IEEE 2nd Global Conference on Advancement in Technology (GCAT); 2021; Bengaluru, India.
3. Bansal S, Prakash K, Sharma K, Sardana N, Kumar S, Gupta N, et al. A highly efficient bilayer graphene/ZnO/silicon nanowire based heterojunction photodetector with broadband spectral response. Nanotechnology. 2020, 31(40): 405205–405205.
4. Bansal S, Prakash K, Gupta A, Kumari M, Patial P, Kaur K, et al. Broadband photodetection through few-layer graphene/ZnO/Si dual-heterojunction and its comparative study with machine learning. In: Advanced Imaging Applications for Interdisciplinary Engineering. Singapore: Bentham Science Publishers Pte. Ltd.; 2026, 17–46.
5. Bansal S, Rajpoot AK, Chamundeswari G, Prakash K, Kumar PR, Rashed ANZ, et al. Pt/ZnO and Pt/few-layer graphene/ZnO Schottky devices with Al ohmic contacts using Atlas simulation and machine learning. Journal of Science: Advanced Materials and Devices. 2024, 9: 100798–100798.
6. Bansal S, Kumar S, Jain A, Rohilla V, Prakash K, Gupta A, et al. Design and TCAD analysis of few-layer graphene/ZnO nanowires heterojunction-based photodetector in UV spectral region. Science Report. 2025, 15: 1–21.
7. Varma T, Sharma S, Periasamy C, Boolchandani D. Performance analysis of Pt/ZnO Schottky photodiode using ATLAS. Journal of Nanoelectronics and Optoelectronics. 2015, 10(6): 761–765.
8. Patel K, Tyagi PK. Multilayer graphene as a transparent conducting electrode in silicon heterojunction solar cells. AIP Advances. 2015, 5: 077165–077165.

9. Das A, Palit M, Paul S, Chowdhury BN, Dutta HS, Karmakar A, et al. Investigation of the electrical switching and rectification characteristics of a single standalone n-type ZnO nanowire/p-Si junction diode. Applied Physics Letters. 2014, 105: 083106–083106.
10. Alshareefi S.J.A., Al-Nafiey A. Graphene and ZnO NPs-enhanced photodetectors based on SiO NWs: Synthesis, characterization, and applications. Results in Optics. 2024, 16: 100690.
11. Liu Y, Liu K, Yang J, Cheng Z, Chen X, Zhu Y, et al. A self-powered flexible UV photodetector based on an individual ZnO-amorphous Ga_2O_3 core-shell heterojunction microwire. Journal of Materials Chemistry C. 2024, 12: 9623–9629.
12. Wang N, Li J, Wang C, Zhang X, Ding S, Guo Z, et al. Improved UV photoresponse performance of ZnO nanowire array photodetector via effective Pt nanoparticle coupling. Nanomaterials. 2024, 14(17): 1442.
13. Boukhoubza I, Achehboune M, Derkaoui I, Apostol M. M, Basyooni M. A, Khenfouch M, Nedelcu L, Enculescu I, Matei E The interface structural, electronic and optical properties of ZnO nanowires/graphene nanohybrid (ZnO NWs/G): experimental and theoretical DFT investigations. Journal of Alloys and Compounds. 2024, 976: 173109.
14. Wang M., Zheng X., Ye X., Liu W., Zhang B., Zhang Z., Zhai R., Ning Y., Li H., Song A. High-performance photodetectors based on semiconducting graphene nanoribbons. Nano Letters. 2024, 24: 165–171.
15. Shen GH, Tandio AR, Hong FCN. Hydrothermally synthesized ultrathin zinc oxide nanowires based field-effect transistors. Thin Solid Films. 2016, 618: 100–106.
16. Zhang A, Zheng G, Lieber CM. General synthetic methods. In: NanoScience and Technology. Springer Science and Business Media Deutschland GmbH; 2016. p. 15–37.
17. Ghoul M, Braiek Z, Brayek A, Assaker IB, Khalifa N, Naceur JB, et al. Synthesis of core/shell ZnO/ZnSe nanowires using novel low cost two-steps electrochemical deposition technique. Journal of Alloys and Compounds. 2015, 647: 660–664.
18. Geng Y, Jeronimo K, Mahzan MABC, Lomax P, Mastropaolo E, Cheung R. Comparison of ZnO nanowires grown on e-beam evaporated Ag and ZnO seed layers. Nanoscale Advances. 2020, 2: 2814–2823.
19. Jung HJ, Lee S, Yu Y, Hong SM, Choi HC, Choi MY. Low-temperature hydrothermal growth of ZnO nanorods on sol-gel prepared ZnO seed layers: optimal growth conditions. Thin Solid Films. 2012, 524: 144–150.
20. Zhan Z, Xu L, An J, Du H, Weng Z, Lu W. Direct catalyst-free chemical vapor deposition of ZnO nanowire array UV photodetectors with enhanced photoresponse speed. Advanced Engineering Materials. 2017, 19: 1700101.
21. Alvi NH, Hassan W ul, Farooq B, Nur O, Willander M. Influence of different growth environments on the luminescence properties of ZnO nanorods grown by the vapor–liquid–solid (VLS) method. Materials Letters. 2013, 106: 158–163.
22. Gautam K, Singh I, Bhatnagar PK, Peta KR. The effect of growth temperature of seed layer on the structural and optical properties of ZnO nanorods. Superlattices and Microstructures. 2016, 93: 101–108.
23. Filip A, Musat V, Tigau N, Polosan S, Pimentel A, Ferreira S, et al. ZnO nanostructures grown on ITO coated glass substrate by hybrid microwave-assisted hydrothermal method. Optik. 2020, 208: 164372.
24. Li MH, Chen JJ, Chen YS, Lin ST, Lin BH, Kuo MY, et al. Development of a broadband photodetector utilizing ZnO nanorods with grating structure fabricated via nanoimprint lithography. Sensors and Actuators A: Physical. 2024, 375: 115530.
25. Shaygan M, Otto M, Sagade AA, Chavarin CA, Bacher G, Mertin W, et al. Low resistive edge contacts to CVD-grown graphene using a CMOS compatible metal. Annals of Physics. 2017, 529(11): 1600410.
26. Wan X, Xu Y, Guo H, Shehzad K, Ali A, Liu Y, et al. A self-powered high-performance graphene/silicon ultraviolet photodetector with ultra-shallow junction: breaking the limit of silicon? npj 2D Materials and Applications. 2017, 1(4): 1–8.
27. Cheng CC, Zhan JY, Liao YM, Lin TY, Hsieh YP, Chen YF. Self-powered and broadband photodetectors based on graphene/ZnO/silicon triple junctions. Applied Physics Letters. 2016, 109(5): 053501–053501.
28. Zhang TF, Wu GA, Wang JZ, Yu YQ, Zhang DY, Wang DD, et al. A sensitive ultraviolet light photodiode based on graphene-on-zinc oxide Schottky junction. Nanophotonics. 2017, 6(5): 1073–1081.
29. Zulfiqar MW, Nisar S, Dastgeer G, Rabeel M, Ghazanfar H, Ali A, et al. 2D material-based infrared photodetectors: recent progress, challenges, and perspectives. Nanoscale. 2025, 17: 17881–17918.
30. Lee H, Kim J. Advances in near-infrared organic photodetectors: molecular design, exciton dynamics, and device integration. Polymers. 2026, 18: 201.
31. Yang M, Gong K, Cui Y, et al. Band engineering and structural-geometrical engineering in 2D/3D van der Waals heterostructures for advanced photodetection and intelligent sensing. Nano-Micro Letters. 2026, 18: 298.

32. Wang N., Liu Y., Li M., Zhao J., Zhang X., Jiang D. Self-powered p-NiO/n-ZnO heterojunction ultraviolet photodetector based on honeycomb nano-mesh structure. Sensors. 2024, 24: 7733.
33. Wang P, Lan Y, Huan C, Luo J, Cai W, Fan J, et al. Recent progress on performance-enhancing strategies in flexible photodetectors: From structural engineering to flexible integration. Materials Science and Engineering: R: Reports. 2023, 156:100759.
34. Tang Q., Tan G., Zhang H., Li H., Xiong Y., Pang D., Ye L., Fang L., Kong C., Li W. Enhanced photoresponse of self-powered ZnO-based photoelectrochemical-type UV photodetectors via Ga-doping for optical communication application. Journal of Alloys and Compounds. 2024, 972: 172864.
35. Ali SM, Noghanian S, Khan ZU, Alzahrani S, Alharbi S, Alhartomi M, Alsulami R. Wearable and Flexible Sensor Devices: Recent Advances in Designs, Fabrication Methods, and Applications. Sensors. 2025, 25(5): 1377.